Variations to Spin Crossover in $[Fe_xZn_{(1-x)}(Me1,3bpp)_2(ClO_4)_2]$ molecular alloys examined by Magnetometry and Single Crystal X-Ray Diffraction

Rosa Diego [a,b], Olivier Roubeau [c], Guillem Aromí [*, a,b]

Email(s): guillem.aromi@qi.ub.es

[a] Departament de Química Inorgànica i Orgànica, Universitat de Barcelona, Martí i Franquès 1-11, 08028 Barcelona, Spain
[b] Institute of Nanoscience and Nanotechnology of the Universitat de Barcelona (IN2UB), 08007 Barcelona, Spain
[c] Instituto de Nanociencia y Materiales de Aragón (INMA) CSIC and Universidad de Zaragoza, Plaza San Francisco s/n, 50009, Zaragoza, Spain

Abstract: Spin crossover (SCO) active solid solutions with formula $[Fe_xZn_{1-x}(Me1,3bpp)_2](ClO_4)_2$ (x = 0.10, 0.15, 0.22, 0.33, 0.41, 0.48, 0.56 and 0.64, Me1,3bpp is a *bis*-pyrazolylpyridine) and the complex $[Zn(Me1,3bpp)_2](ClO_4)_2$ have been prepared and characterized by single crystal X-ray diffraction. The structural data and the powder diffraction patterns of all the compounds have been compared with the reported isostructural molecular crystal $[Fe(Me1,3bpp)_2](ClO_4)_2$. Increasing amounts of Zn diminishes monotonically the cooperativity of the SCO of the parent Fe(II) complex ($T_{1/2}$=183 K) and cause a decrease of $T_{1/2}$ in line with the negative chemical pressure exerted by the Zn(II) complexes on the Fe(II) lattice. The gradual variation of the magnetic properties as the composition changes are paralleled by the evolution of the structural parameters at the molecular, intermolecular and crystal lattice scales. Thermal trapping of a portion of the Fe(II) centers of these alloys by quenching the crystals to 2 K unveils that, upon warming, the temperature of relaxation of the metastable states is almost constant for all compositions.

Keywords: Spin-crossover, Magnetic dilution, Cooperativity, Magneto-structural correlations

I. Introduction

Spin Crossover (SCO) is a molecular local phenomenon that consists of the switching of the magnetic state of transition metal centers caused by a reversible change to the distribution of their *d* electrons [1,2]. Within a pseudo-octahedral environment, this can take place in metal ions with d^4-d^7 configurations. The switching may occur following the influence of an external stimulus, such as temperature or pressure changes or the impact of light irradiation. These properties render such phenomenon very promising in the race for the implementation of switchable devices at the nanoscopic scale for spintronic applications [3]. The SCO property has been mostly studied in octahedral iron (II) complexes [2,4-6]. In this case, the transition toggles the metal center between a magnetic S = 2 high-spin (HS) state and an S = 0 diamagnetic low-spin (LS) state. The case of Fe(II) is also remarkable because the switching is accompanied by a drastic change to the iron-ligand bond distances of 10% or larger [7,8]. In the case of crystalline materials, these changes may propagate through the lattice if the spin active species are connected by intermolecular interactions [9], thus affecting the macroscopic properties [10,11] and conferring cooperativity [12] to the process and even bistability to the system [13]. Salient applications of the bistability within this class of magnetic materials are these related with room temperature data storage by chemically designed molecular architectures [4,14,15]. Predicting the SCO behaviour in terms of thermodynamic parameters and kinetic properties is still a daunting challenge, given the large number of variables playing a role. For the specific

property of cooperativity, some theoretical models have been put forward to rationalize the properties of the spin-change propagation throughout the lattice [16]. From the experimental perspective, synthetic efforts target to influence the type, nature and strength of the interactions between the spin active species (*i.e.* Fe(II) ions). One approach is to link them through extended coordination bonds within 1-, 2- or 3D polymers [14,17-21]. Another pertinent strategy focuses on weak intermolecular interactions like hydrogen bonds [22,23] or π···π stacking interactions connecting the Fe(II) complexes [22,24,25]. In this respect, the specific role of the exact crystal packing of a given set of components can be studied if various polymorphs of a given SCO compound are accessible. These studies are scarce and have revealed the dramatic impact of the specific lattice organization on the various parameters of SCO, including the cooperativity [26-29]. Another interesting way to investigate the cooperativity of SCO molecular materials is through monitoring the effect of doping their lattice with different amounts of spin non-active complexes with the same molecular structure as the active ones. The resulting molecular alloys are isostructural to the parent one. Most studies involve doping a network of Fe(II) complexes with their Zn(II) analogue [30-40], but other metal ions (Mn, Co, Ni or Cd in the oxidation state 2+) have been used for the dopant complex as well [30,36-38,40-46]. The effect of the doping is a decrease of the cooperativity caused by the inclusion of complexes that do not undergo structural changes while the spin active species experience the SCO, thus disrupting its propagation. The dilution also causes a reduction of the temperature of the transition (usually measured as $T_{1/2}$, *i.e.* the temperature at which half of the Fe(II) centers that participate of the SCO have undergone the transition). The decrease of $T_{1/2}$ occurs because the ionic radius of the M(II) center of the dopant, $r(M^{2+})$, is either larger than that of HS Fe(II), ($r(Fe_{HS}^{2+})$ = 78 pm), or in between the latter and that of LS Fe(II), ($r(Fe_{LS}^{2+})$ = 61 pm). The large radius of the dopant causes a negative chemical pressure on the Fe(II) centers of the lattice that encumbers their HS-to-LS transition, effectively stabilizing the HS state. Another effect of the negative chemical pressure is that upon thermal SCO to the LS, the amount of residual HS centers remaining at low temperature increases as the concentration of the dopant is larger. It is well established that the HS state can be generated at low temperature as a trapped metastable excited state following light irradiation of the material when lying in a stable LS state. This process is called light induced excited spin state trapping (LIESST) [47,48]. The metastable HS state may relax back to the LS state within the temperature range where the latter is stable. It is necessary to increase the temperature up to a certain value in order to activate a thermal relaxation regime. The temperature at which this process of relaxation takes place, for a given set of conditions, is called T(LIESST) [49]. The relationship between $T_{1/2}$ and T(LIESST) follows the so-called inverse energy-gap law [50], by which if $T_{1/2}$ gets smaller, T(LIESST) increases [51]. In a related manner, the HS state may also be retained as a metastable state following a very sudden and sufficiently large decrease of temperature in a system lying initially in the HS state [52,53]. This thermal quenching of the HS state is called thermally induced excited spin state trapping (TIESST), while the temperature of the thermal relaxation of the metastable state is called T(TIESST). The dependence of T(LIESST) with the composition of doped SCO molecular crystals has been investigated [33,54]. In the case where the dopant is made of Zn(II) complexes ($r(Zn^{2+})$ = 74 pm), it was observed that, contrary to $T_{1/2}$ (see above), T(LIESST) remains almost unchanged, which contradicts the inverse energy-gap law [33,54]. By contrast, if the metal of the dopant is Ni(II) (with smaller $r(Ni^{2+})$; 69 pm), the increase of dopant leads to a decrease of T(LIESST) [40,46]. On the other hand, doping a lattice of $[Fe(phen)_2(NCS)_2]$ (phen = phenantroline) with Cd(II) complexes ($r(Cd^{2+})$ = 95 pm), which causes a strong decrease of $T_{1/2}$ as a result of the large chemical pressure, does lead to an increase of T(LIESST) [40]. Similarly, an investigation conducted on $[Fe(bpp)_2](BF_4)_2$ (bpp = 2,6−*bis*−pyrazolylpyridine) doped with HS Mn(II), ($r(Mn_{HS}^{2+})$ = 78 pm) revealed a similar behaviour, *ie.* an increase of T(LIESST) with the dopant [36]. These observations underscore the fact that several factors influence the relaxation of the photo-induced metastable state in molecular alloys; *i*) the cooperativity, which is reduced dramatically with the doping, plays a role in propagating the relaxation, *ii*) the inverse energy-gap law is explained with local thermodynamic arguments based on the relation between the potential well of both states, *iii*) the internal chemical pressure caused by the doping plays an important role on the spin transition processes. The influence of the composition of doped Fe(II) lattices on the relaxation of their thermally trapped HS state, specifically on T(TIESST), has been very little explored, although the trends are expected to be the same as for T(LIESST). One of the few cases investigated is that of Mn(II) doped $[Fe(bpp)_2](BF_4)_2$, which reveals indeed that the relaxation of the metastable state produced by thermal quenching exhibits the same tendency as that seen for the photoinduced HS state [45]. However, more studies are necessary in order to confirm this parallelism.

We recently studied the SCO properties of complexes $[Fe(Me1,3bpp)_2](ClO_4)_2$ and $[Fe(2Me1,3bpp)_2](ClO_4)_2$ (Me1,3bpp = 2-(3-methyl-pyrazol-1-yl)-6-(pyrazol-3-yl)pyridine; 2Me1,3bpp = 2-(3,5-dimethyl-pyrazol-1-yl)-6-(pyrazol-3-yl)pyridine, **Figure 1**) to elucidate the effect of the methyl substituents of the bpp core on the parameters of the spin transition and its cooperativity [55].

Both compounds exhibit abrupt SCO processes, at very different temperatures (at $T_{1/2}$ of 184 and 378 K, respectively). In turn, the properties of crystalline solid solutions comprising complexes with both ligands were studied, unveiling an interesting allosteric effect to the SCO [56]. All these compounds being solvent free (*i.e.* their lattice do not include crystallization solvents), they are ideal for studies of solid solutions. Therefore, we prepared a series of solid solutions of complexes $[Fe(Me1,3bpp)_2](ClO_4)_2$ (**1**) and $[Zn(Me1,3bpp)_2](ClO_4)_2$ (**2**) of various compositions described by the formula $[Fe_xZn_{1-x}(Me1,3bpp)_2](ClO_4)_2$ (**3*x***) for x = 0.10, 0.15, 0.22, 0.33, 0.41, 0.48, 0.56 and 0.64). In addition to the pure phases **1** and **2**, the molecular structure of all the composite systems of the series **3*x*** was analysed by single crystal X-ray diffraction (SCXRD), which has allowed to monitor in full detail the structural evolution of the molecular material as the composition gradually changes. This level of structural knowledge is virtually unprecedented in studies of doped SCO crystalline materials. All compounds have also been characterized by inductively coupled plasma-optical emission spectrometry (ICP-OES) and elemental analysis, as well as powder X-ray diffraction (PXRD) and mass spectrometry. The variation of the SCO process of **1** as the amount Zn(II) dopant increases has been analysed by means of bulk magnetization measurements at variable temperature, in light of the structural changes associated to it. All spin active members of this family have been thermally quenched to 2 K, causing the thermal trapping of a small portion of their Fe(II) complexes into a metastable HS state, which then undergoes partial relaxation to the LS state upon warming. The analysis of the dependence of the temperature of relaxation (here determined approximately and called T_{relax}) with the composition is one of the first carried out in SCO doped lattices.

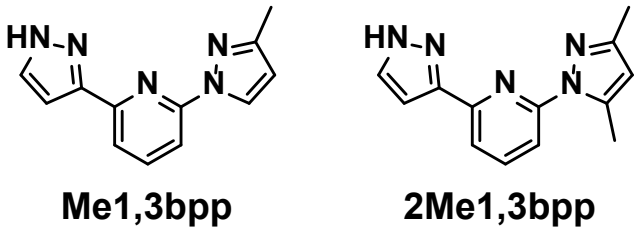

Figure 1. Ligands Me1,3bpp and 2Me1,3bpp.

II. Results and Discussion

Synthesis. The ligand 2-(3-methyl-pyrazol-1-yl)-6-(pyrazol-3-yl)pyridine (Me1,3bpp) and its complex $[Fe(Me1,3bpp)_2](ClO_4)_2$ (**1**) were prepared as previously published by our group [55]. Complex $[Zn(Me1,3bpp)_2](ClO_4)_2$ (**2**) has now been obtained following the same procedure used for **1**, the analogous iron (II) complex, only changing the reaction solvents. Mixing $Zn(ClO_4)_2{\cdot}6H_2O$ with Me1,3bpp in dry acetone produced a colourless solution. Layers of this solution with diethyl ether gave rise to white needles after two days. The solid solutions $[Fe_xZn_{1-x}(Me1,3bpp)_2](ClO_4)_2$ (**3*x***) were obtained through a very similar procedure, by mixing varying ratios of the iron (II) and zinc (II) perchlorate salts. The alloys with lower iron content (x = 0.10, 0.15, 0.22, 0.33) were prepared using dry acetone as a reaction solvent, while the rest of the compositions (x = 0.41, 0.48, 0.56, 0.64) originated from a solvent mixture of dry acetone and ethanol (1/1 vol.). In all cases, yellow, needle-like crystals of a unique phase were obtained following the slow diffusion of diethyl ether into the reaction mixture. Instead, the use of only acetone as solvent when aiming $x > 0.33$ produced non-homogeneous solid phases (**Figure S1**). The fact that complex **1** is obtained with pure ethanol as a solvent prompted the inclusion of the latter as part of the solvent mixture for the mixed-metal compounds richer in Fe(II), yielding the result sought. This difference in the procedure did not influence the solid-state study and its conclusions since all the products were found to be isostructural and free of crystallization solvents (see below). For compositions aimed at $x > 0.64$ the reaction did not produce homogeneous compounds for none of the conditions explored. The crystals from all the reactions with a homogeneous outcome were amenable (see below) to single crystal X-ray diffraction (SCXRD). All compounds (**2** and **3*x***, x = 0.10 to 0.64) were found to be isostructural to **1** with composition $[Fe_xZn_{1-x}(Me1,3bpp)_2](ClO_4)_2$ (**2** or **3*x***). The Fe:Zn ratios of the crystalline samples (**3*x***) were determined by quantitative (ICP-OES) metal trace analysis (**Table S1**) and were consistent with SCXRD data (see below). It was found that the amount of iron found for each isolated crystalline solid (x) is slightly lower than the original iron-to-Zn ratio used experimentally (**Figure 2**), reflecting on the relative thermodynamic

stabilities of the various mixtures in the solid state versus the solution. In fact, there seems to be a change of regime in this ratio when the reaction solvent changes from acetone to the 1:1 mixture of ethanol/acetone. Elemental analysis fit the chemical composition of the crystals of **2** and **3x** considering that they absorb a small amount of water from the atmosphere (< 1 equiv., Table S2). In addition, the positive-ion MALDI MS spectrogram of one of the **3*x*** alloys (x = 0.22) was compared with that of **1** and **2**, respectively. The solid solution furnished the peaks corresponding to each of its individual molecular components at m/z = 505.1 for $[FeC_{24}H_{21}N_{10}]^+$ and m/z = 513.1 for $[ZnC_{24}H_{21}N_{10}]^+$, respectively, exactly at the positions observed for the pure compounds, reproducing the respective isotopic distributions (**Figure S2**). All these observations demonstrate that homogeneous solid solutions of complexes $[Fe(Me1,3bpp)_2](ClO_4)_2$ (**1**) and $[Zn(Me1,3bpp)_2](ClO_4)_2$ (**2**) with a wide range of compositions can be obtained to study the effect of the composition on the key parameters and cooperativity of the SCO of Fe(II).

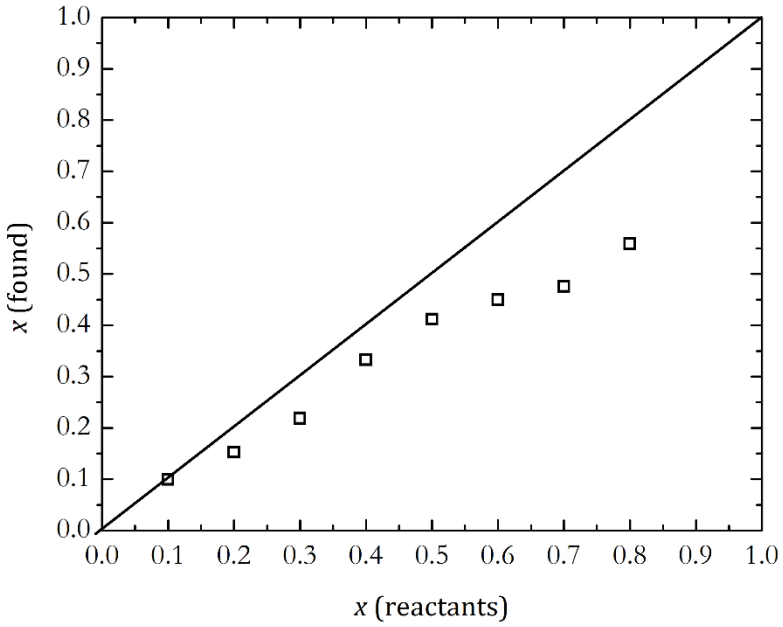

Figure 2. Iron fractions (x) present in the series $[Fe_xZn_{1-x}(Me1,3bpp)_2](ClO_4)_2$ (**3x**) as detected by ICP-OES plotted versus the fractions employed in the reactants for their preparation. The diagonal line is a reference.

Description of the structures

The molecular structure of the complex $[Fe(Me1,3bpp)_2](ClO_4)_2$ (**1**) has been previously reported [55].

$[Zn(Me1,3bpp)_2](ClO_4)_2$ (**2**). Complex **2** is found, at 100 K, in the monoclinic *C2*/c space group. The asymmetric unit consists of one formula unit, with eight such moieties present in the unit cell. The cationic complex, $[Zn(Me1,3bpp)_2]^{2+}$, displays a distorted octahedral Zn(II) center coordinated to two neutral Me1,3bpp *tris*-imine ligands lying approximately perpendicular to each other (**Figure 3**). Since the ligand Me1,3bpp is asymmetric, the complex is chiral and both enantiomers are present in the lattice, which constitutes a racemate. The average of the Zn–N bond distances is 2.16(1) Å, which is consistent with the ionic radius of Zn(II) (r=74 pm), itself closer to the HS iron (II) metal radius (r=78 pm) than the LS counterpart (r=61 pm). The distortion parameters Σ and Θ, which measure the deviation of the coordination geometry from an ideal octahedron [57,58], are 137.1(3) and 445.7(6), respectively. Each cation of **2** interacts with its two ClO_4^- anions *via* hydrogen bonds with the N−H groups of both Me1,3bpp ligands (**Figure 3**). The compound is isostructural with the Fe analogue (**1**); an overlay of both asymmetric units shows only subtle atomic displacements between them (**Figure S3**, **Table S3**).

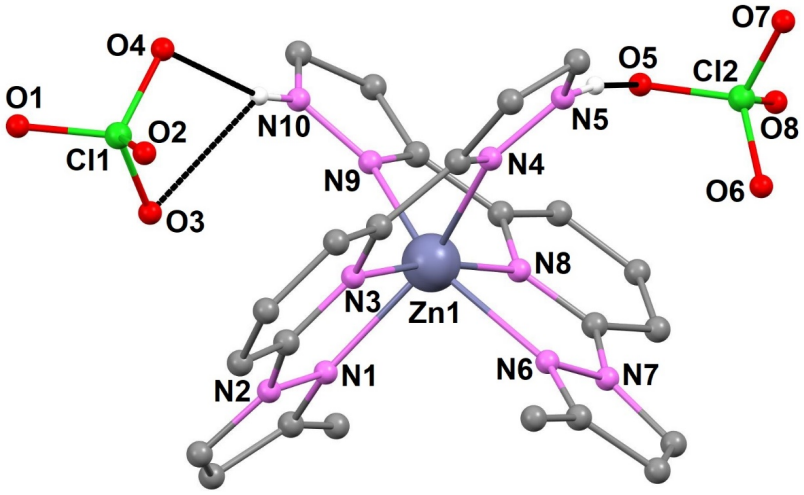

Figure 3. Molecular representation of $[Zn(Me1,3bpp)_2](ClO_4)_2$ (**2**) at 100 K with heteroatoms labelled and C atoms shown in grey. Only H atoms of N–H groups shown (in white). Dashed lines are H-bonds.

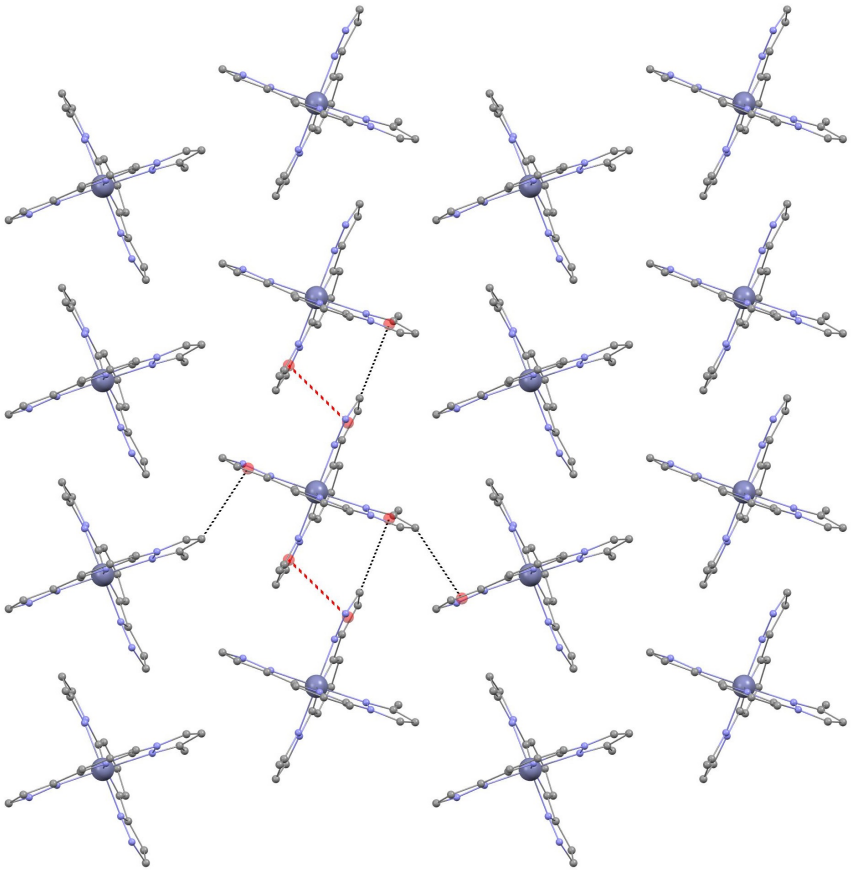

Figure 4. Representation of one sheet of the cationic $[Zn(Me1,3bpp)_2]^{2+}$ complexes of **2**, emphasizing their two different orientations and the main interatomic interactions that one complex establishes with its neighbors; four C−H···π contacts (black dashed lines) and two π···π bonds (red dashed lines). The centroids of the pyrazolyl rings involved are red balls.

The $[Zn(Me1,3bpp)_2]^{2+}$ cations are organized in sheets (**Figures 4** and **S4**), which alternate arrays of cations in two different orientations (with an angle of 41.59°, **Figure S5**) and opposite chirality, as seen before with related Fe(II) complexes [26,55]. Thus, each complex displays the same amount of intermolecular interactions within and between sheets. The former set is established mainly with four first-neighbors (**Figure 4**) in form of two π···π contacts and four C−H···π interactions (see details in **Table S4** and **Figure S4**). In between sheets, weaker C−H···π interactions are established.

$[Fe_xZn_{1-x}(Me1,3bpp)_2](ClO_4)_2$ (3*x*). The structural details of the crystal lattice composing all the solid solutions **3*x*** (x = 0.10, 0.15, 0.22, 0.33, 0.41, 0.48, 0.56, 0.64) were determined by SCXRD at 100 K. The crystals had a pale-yellow colour that fade upon dilution. All the alloys are isostructural among them and with **1** and **2**, displaying very similar cell parameters (see the crystal data in **Table S5**). The simultaneous presence at the position of the metal of both, iron and zinc ions in the averaged model was detected by anomalous thermal parameters at that position. Their precise locations, however, could not be discriminated because of their proximity. The existence of a sole homogeneous crystallographic phase and the presence of only one metal site suggest that both atoms, Fe and Zn, are randomly distributed within the structure. Refinements conducted with free occupancy factors for Fe and Zn at the position of the metal produced best models for Zn/Fe ratios that were close to these determined with metal analysis. In the two cases with largest deviations (x = 0.15 and 0.64), the refinement was likely affected by additional restrains introduced on the reason of further disorder of the perchlorate anions (see details on Supporting Information). In all cases, good quality models were reached (with *R1* and *wR2* typically of 0.04 and 0.09, respectively). By virtue of their isostructural nature, the overall disposition of the components of the alloy within the lattice is the same as in the parent compounds, as are the intermolecular interactions. Most geometric parameters exhibit a detectable gradual evolution from the values observed for one end composition, $[Zn(Me1,3bpp)_2](ClO_4)_2$ (x = 0; **2**) to the other, $[Fe(Me1,3bpp)_2](ClO_4)_2$ (x = 1; **1**), as a result of the progressive substitution of Zn(II) (r = 74 pm) by LS Fe(II) (r = 61 pm). Interestingly, these changes are observed at the atomic, the molecular and the unit cell scales (**Figure S6**), underlying the multiscale dimension that collective local changes within a crystal lattice acquire when the crystal components are connected by intermolecular interactions [10].

Powder X-ray diffraction (PXRD) data were obtained in the range 2θ = 5−60 for all the **3*x*** alloys, as well as for compounds **1** and **2**. In all cases, very sharp signals are observed, confirming the high crystallinity of the phases obtained. All patterns are very similar and exhibit a remarkable continuity in going from one end of the composition spectrum to the other (*ie.* from **1** to **2**, through the successive **3*x*** compositions), confirming that the various $[Fe_xZn_{1-x}(Me1,3bpp)_2](ClO_4)_2$ materials are made of well-defined crystalline solid solutions (**Figure 5**). Since the PXRD measurements were performed at 300 K and the SCXRD determinations took place at 100 K, a direct comparison between experimental and PXRD is not possible. In addition, the Fe centres in these systems are at a different spin state at each of these two temperatures, which is known to vary significantly the diffraction patterns. However, comparison at 300 K (with the Fe centres in the HS state) satisfactorily suits complex **1** [55], and there is continuity of the 300 K spectrograms over the entire range of compositions. The few additional peaks present in all the compounds of the **3*x*** series with respect to both pure compounds are attributed to the effect of the disorder at the perchlorate anion featured by all the members of the series and not by the pure compounds. These observations confirm that the crystal lattice is the correct one and it is maintained for the entire series of compounds studied.

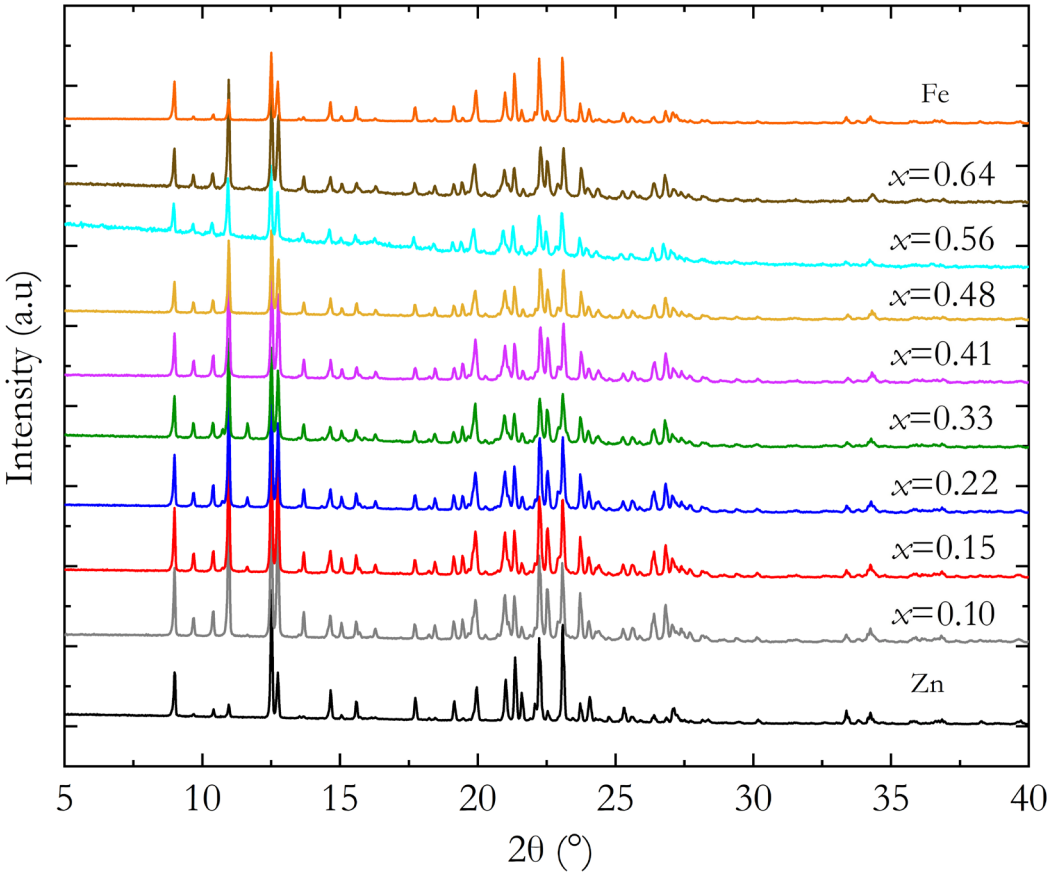

Figure 5. Experimental powder X-ray diffractograms of complexes $[Fe(Me1,3bpp)_2](ClO_4)_2$ (**1**), $[Zn(Me1,3bpp)_2](ClO_4)_2$ (**2**) and solid solutions $[Fe_xZn_{1-x}(Me1,3bpp)_2](ClO_4)_2$ (**3*x***).

Solid-state magnetic properties

The magnetic properties of the series of solid solutions **3*x*** were investigated through variable temperature bulk magnetic susceptibility measurements. Specifically, we were interested on the potential SCO behaviour of the $[Fe(Me1,3bpp)_2](ClO_4)_2$ complex when introduced into the lattice of $[Zn(Me1,3bpp)_2](ClO_4)_2$ (**2**) with increasing concentrations. Polycrystalline samples of the eight compounds were quenched from room temperature to 2 K and then, the magnetization was measured upon warming until 300 K under an external magnetic field of 0.5 T. The data collection was then conducted in the same conditions upon cooling back to 2 K and then upon warming again to 300 K. For all compounds, the data represented in form of χT *vs* T plots (where χ is the molar paramagnetic susceptibility, **Figure 6**, left) show first a jump of χT with the initial warming from 2 K, to reach a plateau until around 74 K, followed by a decline. Upon further warming, a minimum is reached and then a fast increase of χT *vs* T takes place, levelling off around 175 K and staying approximately constant until 300 K. Upon cooling, the χT *vs* T plots follow the inverse path as for the warming until reaching the position of the minimum, below which, this time the decline is succeeded directly by a lower plateau (**Figure 6**, right). The χT *vs* T graph of the subsequent warming cycle (2 → 300 K) superimposes to that of the 300 → 2 K. The initial increase following the first quenching is due to the fact that some of the $[Fe(Me1,3bpp)_2]^{2+}$ species have been thermally trapped in a metastable high-spin (HS) state, subject to zero field splitting effects [59,60] at the lowest temperature. The subsequent decline of χT towards a minimum is due to the thermal relaxation of most of these trapped species to the low-spin (LS) state, stable in this temperature range. The possibility of trapping some of the Fe(II) centers in a metastable HS state at low temperature was the reason for the first initial fast cooling from room temperature to 2 K. The new increase of χT is the thermal LS to HS SCO of the Fe(II) centers. This transition is reversed upon cooling back from 300 K, reaching a plateau at around 80 K with a lower χT value than that obtained following the first

thermal quenching. The molar paramagnetic response of the alloys **3*x*** is proportional to *x*, the fraction content of Fe(II). For example, at 300 K, χT ranges 2.24 to 0.34 cm^3Kmol^{-1} in changing *x* from 0.64 to 0.10 (**Figure 6**).

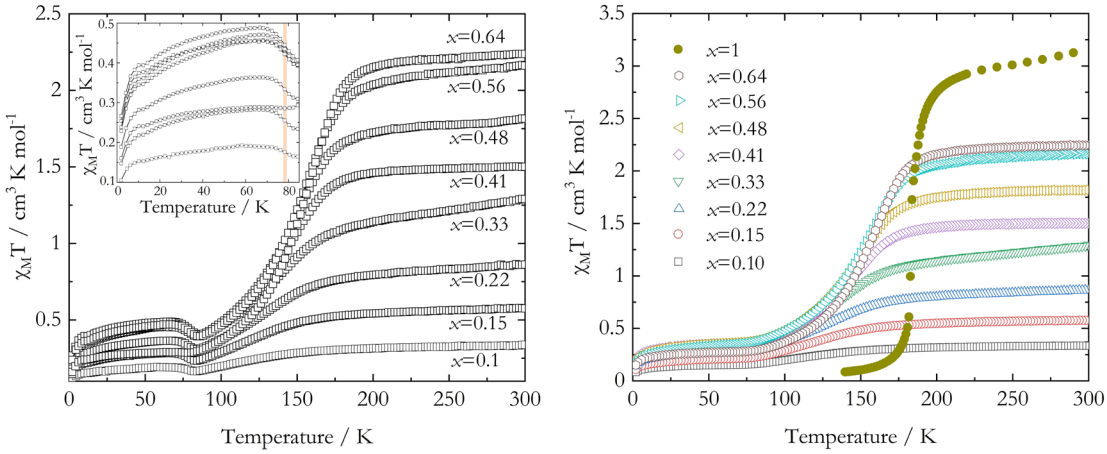

Figure 6. (left) Plots of χT *vs T* for solid solutions $[Fe_xZn_{1-x}(Me1,3bpp)_2](ClO_4)_2$ (**3*x***), measured from 2 K to 300 K after quenching the polycrystalline samples from room temperature. The inset is the part of the plot emphasizing the response of a small portion of Fe(II) trapped in a metastable HS state, following the thermal quenching, that relax to the LS state. The orange band is the narrow range of temperatures containing T_{relax} (the approximate temperature of relaxation) for all compositions. (right) Plots of χT *vs T* for compounds **3*x*** and $[Fe(Me1,3bpp)_2](ClO_4)_2$ (**1**) recorded during the 300 K → 2 K temperature cycle, after the first warming.

From a qualitative inspection of the SCO curves, it is clear that the decrease of Fe(II) concentration within the $[Fe_xZn_{1-x}(Me1,3bpp)_2](ClO_4)_2$ lattice reduces the cooperativity of the SCO, by making the thermal transition more and more gradual (for comparison, the SCO curve of $[Fe(Me1,3bpp)_2](ClO_4)_2$ (**1**) is included in the plots of **Figures 6**, right and **7**, left). This feature is expected and emerges from all the studies of solid solutions made by a SCO active Fe(II) complex together with a non-active isomorphic complex [30-46]. The reason is that the cooperativity of the spin transition relies on the propagation of the structural changes that take place at the molecular level upon SCO. This propagation is ensured by elastic interactions among the switchable complexes. The inclusion of non-active species implies the interposition of complexes that do not undergo these changes, thus diminishing the efficient propagation of the molecular breathing and drastically reducing the cooperativity. To analyse quantitatively this effect, the fraction of Fe(II) centers in the HS state, γ_{HS}, has been derived from the magnetic data above 50 K, *i.e.* a temperature at which the HS-to-LS SCO process is complete. This has been done by normalizing, for each composition, the χT value at a given temperature with those of the fully LS and HS states using the expression $\chi_{HS}(T) = (\chi T(T) - \chi T_{LS}(T))/(\chi T_{HS}(T) - \chi T_{LS}(T))$. This normalization empirically takes into account the effects of ZFS of remaining HS species as well as slight variations in χT due to temperature independent paramagnetism or unideal diamagnetic corrections. The results are shown in **Figure 7**, left. To extract a mean-field estimation of the SCO cooperativity, the phenomenological domain model of Sorai was then fit to the $\gamma_{HS}(T)$ data (**Figure S7**), using the expression (Equation 1),

$$\gamma_{HS}(T) = \gamma_{HS}^{residual} + \frac{\gamma_{HS}^{residual}}{1+e^{\left[\frac{n\Delta_{SCO}H}{R}\left(\frac{1}{T}-\frac{1}{T_{SCO}}\right)\right]}} \quad (1)$$

The model is based on heterophase fluctuations and gives a measure of cooperativity through the number of like-spin molecules (or here the SCO centers), *n*, per interacting domain, the larger the domain the more cooperative the transition [61,62]. This is the same model we have previously used to analyse the effect of doping complex **1** with another SCO-active analogue, $[Fe(2Me1,3bpp)_2](ClO_4)_2$ (**4**) [56], except that here,

the excess enthalpy associated with the SCO process, $\Delta_{SCO}H$, has not been experimentally determined, and therefore we evaluate together the product $n\Delta_{SCO}H$. Also the term $\gamma_{HS}^{residual}$ has been included here to take into account the fraction of Fe(II) ions that remain in their HS state, something that was not necessary for the series **4*x***, in which a allosteric SCO occurred for all Fe(II) centers simultaneously in the solid solutions. Here, as expected, $n\Delta_{SCO}H$ decreases with decreasing x, and would extrapolate to *ca.* 4.4 kJ/mol for infinite dilution, a situation corresponding to isolated SCO centers and thus $n = 1$. An estimation of n using $\Delta_{SCO}H = 4.4$ kJ/mol then actually shows that n is already close to unity for $x = 0.10$. A comparison of the value of $n\Delta_{SCO}H/RT_{SCO}$ derived for the present series **3*x*** with those for the analogue series **4*x*** doping with $[Fe(2Me1,3bpp)_2](ClO_4)_2$ [56] shows a surprisingly good agreement (**Figure 7**, right).

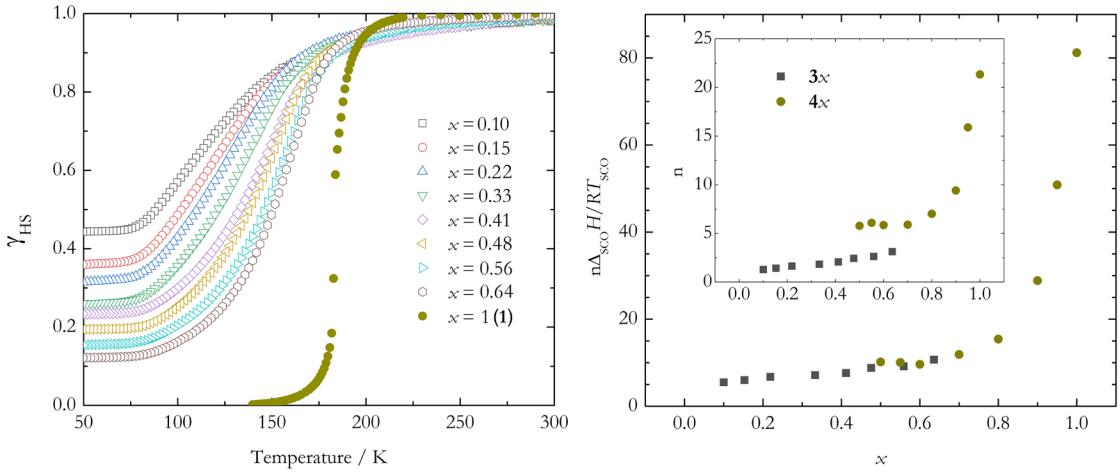

Figure 7. (left) Plots of γ_{HS} *vs.* T for solid solutions $[Fe_xZn_{1-x}(Me1,3bpp)_2](ClO_4)_2$ (**3*x***) and compound $[Fe(Me1,3bpp)_2](ClO_4)_2$ (**1**). (right) Variation of the cooperative character of the SCO for the solid solutions $[Fe_xZn_{1-x}(Me1,3bpp)_2](ClO_4)_2$ (**3*x***), $[Fe(Me1,3bpp)_{2x}(2Me1,3bpp)_{2-2x}](ClO_4)_2$ (**4*x***) and compound $[Fe(Me1,3bpp)_2](ClO_4)_2$ (**1**) as derived through Sorai's domain model (see text).

The comparison allows one to realize that the effect of dilution in the range of x accessible for the **3*x*** series is rather monotonous and relatively weak. Indeed while n has dropped from *ca.* 21 for pure **1** down to *ca.* 3.1 for $x = 0.64$, further dilution only results in a close to linear decrease of n down to *ca.* 1.3 for $x = 0.10$. This is understandable since minimal modifications of the lattice composition upon doping can be expected to have already strong implications on the long-range elastic interaction at the origin of the efficient propagation of the structural modifications associated with the SCO at the molecular scale. A perhaps more surprising and original observation is that this effect seems to be similar whether the doping implies the rupture of some intermolecular interactions among an all-spin-active lattice as in the series **4*x*** or the introduction of spin-inactive centers as in the series **3*x***. It appears that for the same host, different types of doping have a similar destroying effect on the cooperative character of the host SCO process.

Other effects of reducing the concentration of the active complex of the Fe/Zn alloys on the SCO properties of Fe(II) arise from the negative chemical pressure exerted by the Zn(II) complexes on the Fe(II) ones. These are a relative stabilization of the HS state which results in a decrease of the SCO temperature, and the partial hampering of the HS to LS state transition, which induces an increasing residual fraction of Fe(II) ions that remain in the HS state below the SCO temperature [33,36,37,40,42,46]. Both effects are observed here, as seen qualitatively in **Figure 6**, and quantified in **Figure 8**, left. The decrease of T_{SCO} has a linear trend while the residual HS fraction increases more markedly for the lowest x, *i.e.* when T_{SCO} is lowest. The latter may result from the additive effect of increasing Zn content, decreasing T_{SCO} and causing a more gradual SCO, since residual HS fraction are often observed in systems with a gradual SCO process occurring at relatively lower temperatures. Interestingly, this may be contributing to the increase with $\gamma_{HS}^{residual}$ of the average M−N (M=Fe or Zn) bond distances of compounds **3*x*** as determined at 100 K through SCXRD (**Table S5**). To put into perspective the linear

decrease of T_{SCO} observed in the series **3*x***, we have compared the relative decrease ΔT_{SCO}, defined as $T_{SCO}(x)/T_{SCO}(x = 1)$, with four other molecular SCO systems for which doping into the Zn analogue has been studied. These include a similar bis-tris-imine coordination environment in $[Fe_xZn_{1-x}(bpp)_2](NCSe)_2$ (bpp = 2,6-bis(pyrazol-3-yl)pyridine) [53], a *tris*-amineimine chromophore in $[Fe_xZn_{1-x}(2\text{-pic})_3]Cl_2{\cdot}EtOH$ (2-pic = 2-picolylamine) [35] and two systems with axial thiocyanate donors and either a twice *bis*-imine equatorial environment, in $[Fe_xZn_{1-x}(phen)_2(NCS)_2]$ (phen = 1,10-phenantroline) [33], or a tetra-imine chelate, in $[Fe_xZn_{1-x}(bapbpy)(NCS)_2]{\cdot}3DMF$ (bapbpy = N6,N6'-di(pyridin-2-yl)-2,2'-bipyridine-6,6'-diamine) [63].

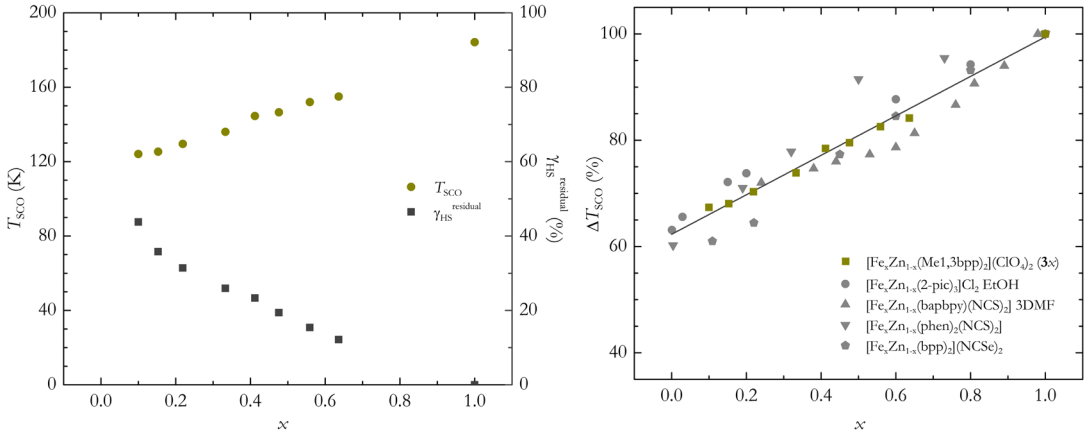

Figure 8. (left) Variation of the spin crossover temperature T_{SCO} for solid solutions $[Fe_xZn_{1-x}(Me1,3bpp)_2](ClO_4)_2$ (**3*x***) together with the values of low temperature $\gamma_{HS}^{residual}$ for all compositions. (right) Relative variation of the spin crossover temperature upon doping for 3x and the series $[Fe_xZn_{1-x}(2\text{-pic})_3]Cl_2{\cdot}EtOH$ (2-pic = 2-picolylamine) [35], $[Fe_xZn_{1-x}(bapbpy)(NCS)_2]{\cdot}3DMF$ (bapbpy = N6,N6'-di(pyridin-2-yl)-2,2'-bipyridine-6,6'-diamine) [63], $[Fe_xZn_{1-x}(phen)_2(NCS)_2]$ (phen = 1,10-phenantroline) [33] and $[Fe_xZn_{1-x}(bpp)_2](NCSe)_2$ (bpp = 2,6-bis(pyrazol-3-yl)pyridine) [53].

Remarkably, and despite different temperature ranges for the SCO as well as different types of SCO processes, the data of all five series of doped materials follow approximately a common master linear trend, best described by $\Delta T_{SCO}(x) = 62.3+37.1x$. The effect of dilution with the spin-inactive ion Zn(II) on the SCO temperature of molecular Fe(II) complexes thus appears to be quite independent of the complex topology/composition, and thus mostly results from the difference in ionic radii. Although this may be surprising, it is in fact in agreement with previous studies that have pointed at a dominant role played by the lattice, the volume change accompanying the spin transition and the associated elastic energies [30]. Indeed, the five molecular SCO systems compared can be expected to have similar lattice (Debye constant) and interaction energies. More rigid 2D or 3D SCO materials may depart from the master linear trend observed here.

Eventually, it was also observed that the thermal relaxation of the small fraction of Fe(II) complexes that are trapped into the HS state upon thermal quenching (**Figure 6** left, inset) occurs at a temperature (termed here T_{relax}) around 77 K, falling for the ensemble of compounds within a very narrow range (approximately 2 K wide). This in contrast with the 40 K range of temperature variation (when x varies from 0.10 to 0.64) observed for $T_{1/2}$ in this series. The models employed to describe the effects of dilution of Fe(II) active complexes when being part of solid solutions associate this $T_{1/2}$ *vs* concentration dependence to a decrease of cooperativity upon dilution. By contrast, the dependence of T(TIESST) or here T_{relax}, with the composition are expected to be much more complex. For the case of T(LIESST) in molecular alloys, this dependence is affected by the decrease of cooperativity as the Fe(II) concentration diminishes, the inverse energy-gap and very importantly, the effect of the internal pressure [33,40,46,54]. In the case of Fe(II)/Zn(II) systems, this results into very little variation of T(LIESST) with the composition. While the relaxation of thermally trapped metastable effects are expected to exhibit a similar behaviour, very few data

are available hitherto [36]. The present data, thus represent one of the first contributions towards the confirmation of this trend.

III. Conclusions

Mixing the salts $Zn(ClO_4)_2$ and $Fe(ClO_4)_2$ with Me1,3bpp in acetone with increasing amounts of the ferrous reagent, produces homogeneous phases of crystalline solid solutions with formula $[Fe_xZn_{1-x}(Me1,3bpp)_2](ClO_4)_2$ (**3*x***; x = 0.10, 0.15, 0.22, 0.33). In this solvent, reactant ratios aiming at x > 0.33 cause the segregation of the crystalline phases, preventing the characterization of any pure compound. However, the solvent medium composed of acetone/ethanol (1:1 in volume) allows increasing the iron content within pure crystalline phases with values of x = 0.41, 0.48, 0.56 and 0.64. Molecular alloys with higher Fe content could not be prepared, perhaps because these are not the thermodynamically preferred option. For all the compositions accessed, SCXRD together with PXRD demonstrate that the alloys are true homogeneous solid solutions. The crystallographic analysis unveils a gradual evolution of the structural parameters with the composition at the local scale, at the level of intermolecular interactions and in terms of the crystal lattice parameters. In light of the structural information, the effect of the composition within these lattices on the cooperativity and the thermodynamic parameters of the SCO of the Fe(II) complexes could be analysed. The effect of the negative chemical internal pressure exerted by the Zn(II) complexes becomes evident with a decrease of $T_{1/2}$ of the SCO and the presence of larger amounts of residual HS Fe(II) centers following the thermal HS to LS transition. Interestingly, the variation of $T_{1/2}$ seems independent of the complex studied as long as the metal of the dopant is the same (when comparing the variation in terms of $\Delta T_{SCO}(x) = T_{SCO}(x)/T_{SCO}(x = 1)$). In addition, the disruption of the network of interactions between spin active species caused by the intercalation of spin passive complexes results in a decrease of the cooperativity. At the highest accessible Fe concentration (x =0.64), it appears that the major disruption of cooperativity has already taken place, so that the variation of cooperativity (gauged here by the expression $n\Delta_{SCO}H/RT_{SCO}$ based on the Sorai model) is weak and linear. Interestingly, this variation for a given SCO lattice (complex **1**) seems independent of the nature of the dopant complex. Interestingly, a small amount of Fe(II) can be trapped thermally in the HS state upon rapid thermal quenching to 2K of the system while initially in the HS state at room temperature. This allows to determine T(ITIESST) temperatures for the various values of x, which provides rare experimental evidence that these relaxation temperatures experience almost no changes with the composition of the doped system, following the same trend as observed for T(LIESST) on Zn(II) doped Fe(II) SCO molecular crystals.

IV. Additional Information

Supporting information is available online. Correspondence and requests for materials should be addressed to corresponding author.

V. Materials and Methods

Synthesis. All reagents were purchased from commercial sources and used without further purification. Ligand 2-(3-metyl)-pyrazol-1-yl)-6-(pyrazol-3-yl)pyridine (Me1,3bpp) and the complex $[Fe(Me-1,3bpp)_2](ClO_4)_2$ (**1**) were prepared as previously reported [55]. **Caution**: Perchlorates salts are potentially explosive. Only small amounts of reagents should be handled, and extreme care must be exerted.

$[Zn(Me1,3bpp)_2](ClO_4)_2$ (**2**). To a solution of $Zn(ClO_4)_2{\cdot}6H_2O$ (12 mg, 0.03 mmol) in acetone (10 ml) was added dropwise a solution of Me1,3bpp (13.5 mg, 0.06 mmol) in acetone (10ml). The resulting colourless solution was stirred for 40 minutes at room temperature. The solution was then filtered and layered with diethyl ether (1:1 vol). Colourless needles of the product suitable for single crystal X-ray diffraction were obtained after a week. Yield: 40%. Anal. Calcd (found) for $ZnC_{24}H_{22}Cl_2N_{10}O_8$: C, 39.96 (40.63); H, 3.18 (3.30); N, 19.41 (18.74).

$[Fe_xZn_{1-x}(Me1,3bpp)_2](ClO_4)_2$ (**3*x***; $0.10<x<0.33$). Depending on the dilution degree x, various quantities of $Fe(ClO_4)_2{\cdot}6H_2O$ and $Zn(ClO_4)_2{\cdot}6H_2O$ (in mg, using the Fe/Zn format, 3.2/41.7, 6.3/36.9, 9.5/32.3

and 12.6/27.7 for x = 0.10, 0.15, 0.22 and 0.33, respectively) and ascorbic acid (~2 mg) were dissolved in acetone (20 ml). A solution of Me1,3bpp (56 mg, 0.25 mmol) in acetone (20 ml) was added dropwise to each metal mixture solution. The resulting yellow solutions were stirred for 45 minutes at room temperature. The solutions were then filtered and layered with diethyl ether (1:1 vol). Yellow needles of the products suitable for single crystal X-ray diffraction were obtained in a week. Typical yields: ~ 39 %. Anal. Calcd (found) for $[Fe_{0.10}Zn_{0.9}(C_{12}H_{11}N_5)_2](ClO_4)_2$: C, 39.7 (40.27); H, 3.24 (3.16); N, 19.29(18.71). Anal. Calcd (found) for $[Fe_{0.15}Zn_{0.847}(C_{12}H_{11}N_5)_2](ClO_4)_2$: C, 39.66 (40.39); H, 3.26 (3.2); N, 19.27 (18.54). Anal. Calcd (found) for $[Fe_{0.22}Zn_{0.781}(C_{12}H_{11}N_5)_2](ClO_4)_2$: C, 39.75 (40.53); H, 3.25 (3.19); N, 19.31 (18.53). Anal. Calcd (found) for $[Fe_{0.33}Zn_{0.667}(C_{12}H_{11}N_5)_2](ClO_4)_2$: : C, 40.27 (40.51); H, 3.16 (3.19); N, 19.56 (19.32).

$[Fe_xZn_{1-x}(Me1,3bpp)_2](ClO_4)_2$ (**3*x***; 0.41<x<0.64). Depending on the dilution degree x, various quantities of $Fe(ClO_4)_2{\cdot}6H_2O$ and $Zn(ClO_4)_2{\cdot}6H_2O$ (in mg, using the Fe/Zn format, 15.8/23.1, 19/18.5, 22.1/13.8 and 25.3/9.2 for x = 0.41, 0.48, 0.56 and 0.64, respectively) and ascorbic acid (~2 mg) were dissolved in a mixture of ethanol and acetone (1:1 vol; 20 ml). A solution of Me1,3bpp (56 mg, 0.25 mmol) in acetone (20 ml) was added dropwise to the former metal mixture solution. The resulting yellow solutions were stirred for 45 minutes at room temperature. The solutions were then filtered and layered with diethyl ether (1:1 vol). Yellow needles of the products suitable for single crystal X-ray diffraction were obtained in a week. Typical yields: ~ 39 %. %. Anal. Calcd (found) for $[Fe_{0.41}Zn_{0.558}(C_{12}H_{11}N_5)_2](ClO_4)_2$: C, 40.2 (40.46); H, 3.19 (3.15); N, 19.53 (19.27). Anal. Calcd (found) for $[Fe_{0.48}Zn_{0.524}(C_{12}H_{11}N_5)_2](ClO_4)_2$: C, 40.32 (40.51); H, 3.18 (3.14); N, 19.59 (19.4). Anal. Calcd (found) for $[Fe_{0.56}Zn_{0.441}(C_{12}H_{11}N_5)_2](ClO_4)_2$: C, 40.04 (40.35); H, 3.24 (3.16); N, 19.45 (19.14). Anal. Calcd (found) for $[Fe_{0.64}Zn_{0.364}(C_{12}H_{11}N_5)_2](ClO_4)_2$: C, 40.46 (40.74); H, 3.17 (3.13); N, 19.66 (19.38).

Elemental Analysis. C, H and N analyses were performed by using a Thermo EA Flash 2000 (Thermo Scientific) analyser at the Centres Científics i Tecnològics from the Universitat de Barcelona (CCiT-UB). Fe and Zn analysis of each sample were performed by inductively coupled plasma-optical emission spectrometry (ICP-OES) with a Perkin Elmer (Optima 3200rl) instrument in standard conditions at the CCiTUB. The Teflon reactor was cleaned with HNO_3 1%. Chemical solutions were prepared from 0.005 g of sample and treated with HNO_3 (3 ml) and H_2O_2 (1 ml) at 90°C overnight. The sample were cooled down and 45 ml of H_2O were added.

MALDI-TOF Mass Spectrometry. Positive-ion (MALDI (Matrix Assisted Laser Desorption Ionization) MS measurements were performed by using a 400 ABSciex MALDI-TOF spectrometer at the Unitat d'Espectrometria de Masses de Caracterització Molecular (CCiTUB), on a MeOF solution. DCTB (trans-2-[3-(4-tert-butylphenyl)-2-methyl-2-propenyli-dene]malononitrile) matrix was added before injection.

Single Crystal X-ray diffraction (SCXRD). Crystallographic data for **2** and the **3** series were collected on a Bruker APEX II QUAZAR diffractometer equipped with a microfocus multilayer monochromator with Mo Kα (λ=0.71973 Å), at 100 K for all complexes. All structures were solved and refined by using the SHELXT [64] and SHELXL [65] programs and the graphical interface Olex2 [66]. The metal diluted structures were firstly solved with only one metal Zn(II) and the Fe(II) metallic centre was introduced to refine the final metal mixed complex. In the resulting structures, the Zn and Fe atoms occupy exactly the same positions. A positional disorder was considered in the "shared" atomic site with the higher electronic density. The refinement was extremely sensitive to this disorder. SIMU and DELU restrictions did not allow to refine properly the disorder and it was impossible to distinct two different positions for each metal centers regarding the close proximity of them. Thus, the same thermic anisotropic movement was enforced for both metallic centres by using the EADP Zn1 Fe1 and EXYZ Zn1 Fe1 constrains. Consequently, Zn and Fe atoms are equivalent and the free refinement of the occupancy factor of each metal allows to confirm the Zn/Fe ratio of each sample. Tables S3, S4 and S5 and Figure S6 gather relevant crystallographic information. All details can be found in CCDC (2096270, x = 0.10; 2096280, x = 0.15; 2096271, x = 0.22; 2096269, x = 0.33; 2096276, x = 0.41; 2096281, x = 0.48; 2096278, x = 0.56; 2096279, x = 0.64; 2096285, **2**) that contain the supplementary crystallographic data for this paper. These data can be obtained free of charge from The Cambridge Crystallographic Data Center via https://summary.ccdc.cam.ac.uk/structure-summary-form.

Powder X-ray diffraction (PXRD). Powder X-ray diffraction data were collected on a PANalytical X'Pert PRO MPD θ/θ powder diffractometer of 240 mm radius at room temperature with Cu Kα radiation (λ = 1.5418 Å) at the Centres Científics i Tecnològics from the Universitat de Barcelona (CCiT-UB). The samples were sandwiched between films of polyester *mylar* of 3.6 microns of thickness. Collection of two 2θ/θ scans from 2 to 60º (2θ) with a step size of 0.0263º and a measuring time of 300 seconds per step were performed with working power of 45 kV – 40 mA.

Magnetic measurements. Magnetic measurements were performed with a MPMS5 SQUID magnetometer at the Unitat de Mesures Magnètiques of the Universitat de Barcelona. The applied magnetic field was 0.5 T. Correction of the diamagnetic contribution of the sample was done using Pascal's constants [67]. Additionally, the diamagnetic contribution of the zinc was corrected. All samples were quenched directly from room temperature to 5 K in the absence of a magnetic field and then, the temperature was reduced to 2 K and stabilized before the measurements for 10 min to ensure thermalization. Then, a 0.5 T magnetic field was applied and the magnetic susceptibility was determined. The temperature scans form 2 K to 300 K and the cooling mode were varied at 1 K/min in 2 K increments.

VI. Conflict of Interests

The authors must declare if there are conflict of interests.

VII. Acknowledgements

The authors thank the Spanish MICINN for grants PGC2018-098630-B-I00 (GA and RD) and MAT2017-86826-R (OR) and the Generalitat de Catalunya for the ICREA Academia 2018 Prize (GA).

VIII. References

[1] Ribas Gispert J. *Coordination Chemistry*. Wiley-VCH: Weinheim, **2008**.

[2] Halcrow M. A. *Spin-Crossover Materials: Properties and Applications*. Wiley: West Sussex, UK, **2013**.

[3] Bousseksou A., Molnar G., Salmon L., Nicolazzi W., *Chem. Soc. Rev.*, **2011**, *40*, 3313-3335.

[4] Gamez P., Costa J. S., Quesada M., Aromí G., *Dalton Trans.*, **2009**, 7845-7853.

[5] Gütlich P., Hauser A., Spiering H., *Angew. Chem., Int. Ed.*, **1994**, *33*, 2024-2054.

[6] Gütlich P., Gaspar A. B., Garcia Y., *Beilstein J. Org. Chem.*, **2013**, *9*, 342-391.

[7] Halcrow M. A., *Chem. Soc. Rev.*, **2011**, *40*, 4119-4142.

[8] Craig G. A., Roubeau O., Aromí G., *Coord. Chem. Rev.*, **2014**, *269*, 13-31.

[9] Spiering H. Elastic Interaction in Spin-Crossover Compounds. In: Gütlich P., Goodwin H.A. (eds). *Spin Crossover in Transition Metal Compounds III*. Springer Berlin Heidelberg: Berlin, Heidelberg, **2004**, pp 171-195.

[10] Guionneau P., Marchivie M., Chastanet G., *Chem., Eur. J.*, **2021**, *27*, 1483-1486.

[11] Guionneau P., *Dalton Trans.*, **2014**, *43*, 382-393.

[12] Nicolazzi W., Bousseksou A., *C. R. Chim.*, **2018**, *21*, 1060-1074.

[13] Halcrow M. A., *Chem. Lett.*, **2014**, *43*, 1178-1188.

[14] Kahn O., *Science*, **1998**, *279*, 44-48.

[15] Larionova J., Salmon L., Guari Y., Tokarev A., Molvinger K., Molnár G., Bousseksou A., *Angew. Chem., Int. Ed.*, **2008**, *47*, 8236-8240.

[16] Popa A.-I., Stoleriu L., Enachescu C., *J. Appl. Phys.*, **2021**, *129*, 131101.

[17] Real J. A., Gaspar A. B., Muñoz M. C., *Dalton Trans.*, **2005**, 2062.

[18] Roubeau O., *Chem., Eur. J.*, **2012**, *18*, 15230-15244.

[19] Weber B., *Coord. Chem. Rev.*, **2009**, *253*, 2432-2449.

[20] Halder G. J., Kepert C. J., Moubaraki B., Murray K. S., Cashion J. D., *Science*, **2002**, *298*, 1762-1765.

[21] Gass I. A., Batten S. R., Forsyth C. M., Moubaraki B., Schneider C. J., Murray K. S., *Coord. Chem. Rev.*, **2011**, *255*, 2058-2067.

[22] Wannarit N., Roubeau O., Youngme S., Teat S. J., Gamez P., *Dalton Trans.*, **2013**, *42*, 7120-1730.

[23] Leita B. A., Moubaraki B., Murray K. S., Smith J. P., *Polyhedron*, **2005**, *24*, 2165-2172.

[24] Barrios L. A., Peyrecave-Lleixa E., Craig G. A., Roubeau O., Teat S. J., Aromí G., *Eur. J. Inorg. Chem.*, **2014**, 6013-6021.

[25] Arcis-Castíllo Z., Zheng S., Siegler M. A., Roubeau O., Bedoui S., Bonnet S., *Chem., Eur. J.*, **2011**, *17*, 14826-14836.

[26] Bartual-Murgui C., Codina C., Roubeau O., Aromí G., *Chem., Eur. J.*, **2016**, *22*, 12767-12776.

[27] Bartual-Murgui C., Diego R., Vela S., Teat S. J., Roubeau O., Aromí G., *Inorg. Chem.*, **2018**, *57*, 11019-11026.

[28] Bartual-Murgui C., Piñeiro-López L., Valverde-Muñoz F. J., Muñoz M. C., Seredyuk M., Real J. A., *Inorg. Chem.*, **2017**, *56*, 13535-13546.

[29] Tao J., Wei R.-J., Huang R.-B., Zheng L.-S., *Chem. Soc. Rev.*, **2012**, *41*, 703-737.

[30] Adler P., Wiehl L., Meibner E., Köhler C. P., Spiering H., Gütlich P., *J. Phys. Chem. Solids*, **1987**, *48*, 517-525.

[31] Jung J., Schmitt G., Wiehl L., Hauser A., Knorr K., Spiering H., Gütlich P., *Z. Phys. B Condens. Matter.*, **1996**, *100*, 523-534.

[32] Buchen T., Poganiuch P., Gütlich P., *J. Chem. Soc., Dalton Trans.*, **1994**, 2285-2288.

[33] Baldé C., Desplanches C., Wattiaux A., Guionneau P., Gütlich P., Létard J.-F., *Dalton Trans.*, **2008**, 2702-2707.

[34] Jakobi R., Spiering H., Wiehl L., Gmelin E., Gütlich P., *Inorg. Chem.*, **1988**, *27*, 1823-1827.

[35] Gütlich P., Link R., Steinhaeuser H. G., *Inorg. Chem.*, **1978**, *17*, 2509-2514.

[36] Baldé C., Desplanches C., Gütlich P., Freysz E., Létard J. F., *Inorg. Chim. Acta*, **2008**, *361*, 3529-3533.

[37] Zhong Y., Takayoshi K.-S., Hiroaki K., Takashi O., Masahiko M., Megumu M., *Bull. Chem. Soc. Jpn.*, **2009**, *82*, 333-337.

[38] Rotaru A., Dîrtu M. M., Enachescu C., Tanasa R., Linares J., Stancu A., Garcia Y., *Polyhedron*, **2009**, *28*, 2531-2536.

[39] Lefter C., Tricard S., Peng H., Molnár G., Salmon L., Demont P., Rotaru A., Bousseksou A., *J. Phys. Chem. C*, **2015**, *119*, 8522-8529.

[40] Sylla M. S., Baldé C., Daro N., Desplanches C., Marchivie M., Chastanet G., *Eur. J. Inorg. Chem.*, **2018**, 297-304.

[41] Sanner I., Meissner E., Köppen H., Spiering H., Gütlich P., *Chem. Phys.*, **1984**, *86*, 227-233.

[42] Ganguli P., Gütlich P., Mueller E. W., *Inorg. Chem.*, **1982**, *21*, 3429-3433.

[43] Martin J.-P., Zarembowitch J., Dworkin A., Haasnoot J. G., Codjovi E., *Inorg. Chem.*, **1994**, *33*, 2617-2623.

[44] Martin J.-P., Zarembowitch J., Bousseksou A., Dworkin A., Haasnoot J. G., Varret F., *Inorg. Chem.*, **1994**, *33*, 6325-6333.

[45] Paradis N., Chastanet G., Létard J.-F., *Eur. J. Inorg. Chem.*, **2012**, 3618-3624.

[46] Baldé C., Desplanches C., Létard J.-F., Chastanet G., *Polyhedron*, **2017**, *123*, 138-144.

[47] Decurtins S., Gütlich P., Kohler C. P., Spiering H., Hauser A., *Chem. Phys. Lett.*, **1984**, *105*, 1-4.

[48] Chastanet G., Desplanches C., Baldé C., Rosa P., Marchivie M., Guionneau P., *Chem. Sq.*, **2018**, *2, 2*.

[49] Létard J.-F., Guionneau P., Rabardel L., Howard J. A. K., Goeta A. E., Chasseau D., Kahn O., *Inorg. Chem.*, **1998**, *37*, 4432-4441.

[50] Hauser A., *Coord. Chem. Rev.*, **1991**, *111*, 275-290.

[51] Létard J.-F., Guionneau P., Nguyen O., Costa J. S., Marcén S., Chastanet G., Marchivie M., Goux-Capes L., *Chem., Eur. J.*, **2005**, *11*, 4582-4589.

[52] Craig G. A., Costa J. S., Roubeau O., Teat S. J., Aromí G., *Chem., Eur. J.*, **2011**, *17*, 3120-3127.

[53] Marchivie M., Guionneau P., Létard J. F., Chasseau D., Howard J. A. K., *J. Phys. Chem. Solids*, **2004**, *65*, 17-23.

[54] Baldé C., Desplanches C., Le Gac F., Guionneau P., Létard J.-F., *Dalton Trans.*, **2014**, *43*, 7820.

[55] Bartual-Murgui C., Vela S., Darawsheh M., Diego R., Teat S., Roubeau O., Aromí G., *Inorg. Chem. Front.*, **2017**, *4*, 1374-1383.

[56] Bartual-Murgui C., Perez-Padilla C., Teat S. J., Roubeau O., Aromí G., *Inorg. Chem.*, **2020**, *59*, 12132-12142.

[57] Guionneau P., Marchivie M., Bravic G., Létard J.-F., Chasseau D., *J. Mater. Chem.*, **2002**, *12*, 2546-2551.

[58] Marchivie M., Guionneau P., Létard J.-F., Chasseau D., *Acta Cryst. B*, **2005**, *61*, 25-28.

[59] Craig G. A., Costa J. S., Teat S. J., Roubeau O., Yufit D. S., Howard J. A. K., Aromí G., *Inorg. Chem.*, **2013**, *52*, 7203-7209.

[60] Halcrow M. A., *Chem. Soc. Rev.*, **2008**, *37*, 278-289.

[61] Sorai M., Seki S., *J. Phys. Chem. Solids*, **1974**, *35*, 555-570.

[62] Sorai M., *Top. Curr. Chem.*, **2004**, *235*, 153-170.

[63] Zheng S., Siegler M. A., Sánchez Costa J., Fu W.-T., Bonnet S., *Eur. J. Inorg. Chem.*, **2013**, 1033-1042.

[64] Sheldrick G., *Acta Cryst. A*, **2015**, *71*, 3-8.

[65] Sheldrick G., *Acta Cryst. C*, **2015**, *71*, 3-8.

[66] Dolomanov O.V., Bourhis L. J., Gildea R. J., Howard J. A. K., Puschman H., *J. Appl. Cryst.*, **2009**, *42*, 339-341.

[67] Bain G. A., Berry J. F., *J. Chem. Educ.*, **2008**, *85*, 532.

Received: 23 July 2021
Accepted: 02 September 2021
Published online: 13 September 2021

ORCID for authors
Guillem Aromí: 0000-0002-0997-9484
Olivier Roubeau: 0000-0003-2095-5843